The root system architecture of wheat establishing in soil is associated with varying elongation rates of seminal roots: quantification using 4D MRI

D. Pflugfelder[1], d.pflugfelder@fz-juelich.de, OrcidID: 0000-0001-6187-2935
J. Kochs[1], j.kochs@fz-juelich.de, OrcidID:
R. Koller[1], r.koller@fz-juelich.de, OrcidID: 0000-0001-7251-7242
S. Jahnke[1,2], s.jahnke@fz-juelich.de, OrcidID: 0000-0002-4086-2567
C. Mohl[1], carola.mohl@gmx.de, OrcidID:
S. Pariyar[1], s.pariyar@fz-juelich.de, OrcidID: 0000-0001-5841-5696
H. Fassbender[1], h.fassbender@fz-juelich.de, OrcidID: 0000-0003-1731-4252
K.A. Nagel[1], k.nagel@fz-juelich.de, OrcidID: 0000-0003-3025-0388
M. Watt[1,3], watt.m@unimelb.edu.au, OrcidID: 0000-0001-7843-0957
D. van Dusschoten[1], d.van.dusschoten@fz-juelich.de, OrcidID: 0000-0002-6251-1231

[1]Forschungszentrum Jülich GmbH, IBG-2: Plant Sciences, 52425 Jülich, Germany;
[2]University of Duisburg-Essen, Biodiversity, Universitätsstr. 5, 45141 Essen, Germany;
[3]School of BioSciences, Faculty of Science, University of Melbourne, Parkville, Victoria, Australia 3010

#corresponding author: d.pflugfelder@fz-juelich.de

Highlight:

Root phenotyping in soil with high temporal resolution revealed the importance of time points of root initiation and elongation rates for the root system architecture of wheat seedlings.

Abstract: Seedling establishment is the first stage of crop productivity, and root phenotypes at seed emergence are critical to a successful start of shoot growth as well as for water and nutrient uptake. In this study, we investigate seedling establishment in winter wheat utilizing a newly developed workflow based on magnetic resonance imaging (MRI). Using the eight parents of the NIAB MAGIC (Multi-parent Advanced Generation Inter-Cross) population we analyzed the 4D root architecture of 288 individual seedlings grown in natural soils with plant neighbors over 3 days of development. Time of root and shoot emergence, total length, angle and depth of the axile roots varied significantly among these genotypes. The temporal data resolved rates of elongation of primary roots and first and second seminal root pairs. Genotypes with slow primary roots had fast first and second seminal root pairs and vice versa, resulting in variation in root system architecture mediated not only by root angle but also by initiation and relative elongation of axile roots. We could demonstrate that our novel MRI workflow with a unique planting design and automated measurements allowed medium throughput phenotyping of wheat roots in 4D and could give new insights into regulation of root system architecture.

Keywords: agriculture, breeding, MRI, NIAB MAGIC population, NMR, phenotyping, seedling establishment, wheat

Introduction

Seedling establishment is the first stage of crop growth and productivity. The root system growth and distribution through the soil in space and time (root system architecture, RSA) influences successful establishment. RSA is determined by three developmental processes: root number, root elongation and root angle (orientation). Root number (Perkins and Lynch, 2021) and root length are associated with nutrient uptake (Palta and Watt, 2009). Root system growth rate influences establishment in farming systems with different amounts of soil ploughing (Watt *et al.*, 2005). Previous studies have associated root growth angles with functions. For example, shallow root angle of bean was associated with shallow P uptake in the field (Henry *et al.*, 2010). In large rhizoboxes and growth to yield, narrow root angle of wheat cv. SeriM82 was associated with deeper water uptake than wider angled barley cv. Mackay (Manschadi *et al.*, 2006). RSA is therefore an important breeding target for improvement of seedling establishment of plants, including major stable crops such as wheat (Ober *et al.*, 2021). RSA depends on plant genes and the soil environment (Lynch, 1995; Rich and Watt, 2013), and phenotyping is a critical component of breeding for better establishment.

Root phenotyping, the quantification of expressed and observable root traits, is an approach that is widely used towards identifying genetic variation to be exploited in breeding, or managed with agronomy (Tracy *et al.*, 2020). Root phenotyping at seedling stages over time has often been done in conditions that constrain root systems to a narrow volume in two dimensions (2D): for example, in agar (Nagel *et al.*, 2020), on germination paper (Gioia *et al.*, 2016), and in rhizotrons (Nagel *et al.*, 2012), or in soil-less conditions (e.g., hydroponics (Tuberosa *et al.*, 2002); aeroponics (De Dorlodot *et al.*, 2005)). The 2D and soil-less methods that take repeated images over time can resolve numbers, rates and angles of individual roots, however, they do not always relate strongly to root system depth and distribution in fields (e.g., Rich *et al.*, 2020). Root phenotyping of whole root systems grown unconstrained in fields most often relies on a harvest and washing followed by measurement: for example, after growth in planted baskets (Uga *et al.* 2011) or after removal with shovelomics (Trachsel *et al.* 2011). 3D field methods can be done at a high throughput (York and Lynch, 2015), however they do not resolve changes in growth of root tips over time, and other quantitative traits

underlying RSA that help to speed up selection in breeding. This gap could be bridged using controlled conditions as there is evidence that young root phenotypes there relate well to young root expression in the field (Watt *et al.*, 2013).

Visualizing the dynamic development of complete root systems in natural soils is currently only possible using X-ray computed tomography (CT; Mooney *et al.*, 2012; Flavel *et al.*, 2012), magnetic resonance imaging (MRI; van Dusschoten *et al.*, 2016) or neutron tomography (Mawodza *et al.*, 2020). X-ray CT and MRI generate spatial and time resolved data that can reveal quantitative traits such as growth rates and allocation patterns to growth of roots and shoots (Atkinson *et al.*, 2019). Due to measurement times and cost constraints, these methods are often used at low throughput measuring the time courses of typically less than 40 plants per study (Blaser *et al.*, 2018; Flavel *et al.*, 2012; Tracy *et al.*, 2012; Blunk *et al.*, 2017; van Dusschoten *et al.*, 2016; Metzner *et al.*, 2015; Pflugfelder *et al.*, 2017; Khalil *et al.*, 2020, van Harsselaar *et al.*, 2021). These numbers are insufficient for applications in pre-breeding and agronomic practices.

Here we present a non-invasive, automated approach to quantify RSA phenotypes at plant establishment, in soil in 4D with neighboring plants. We used MRI to quantify roots and coleoptiles emerging from soil over time. MRI images hydrogen atoms in the root-soil sample using magnetic fields and radio waves. MRI has been used clinically for over three decades without serious side effects (ICNIRP, 2017). In particular, it does not employ ionizing radiation. Ionizing radiation as needed for X-Ray CT or neutron tomography can have an effect on plant growth such as root growth rates (Clowes and Hall, 1963). MRI is thus advantageous for repeated measures to obtain rates of root growth and dynamics of RSA formation over time. Recently MRI was shown to function across different soil types: The seminal axile roots of barley seedlings were resolved in seven soils and their branch roots (to 0.3 mm diameter) in five soils (Pflugfelder *et al.*, 2017).

We used wheat (*Triticum aestivum* L.) to establish a non-invasive phenotyping workflow using MRI. Wheat is of major importance to global food security (Shiferaw *et al.*, 2013), and spans the widest range of pedoclimatic zones of all crops. The recent availability of a fully annotated reference genome

for wheat (Consortium, 2018) is expected to fuel improvements in wheat productivity which requires linking genetic information to phenotypic data. To this end Multi-parent Advanced Generation Inter-Cross (MAGIC) populations were developed by inter-crossing multiple parental lines in a balanced funnel crossing scheme which have high allelic diversity, high levels of recombination, and the genomes form a fine-scale mosaic of all the parents (Huang *et al*., 2015). Here, we phenotyped the eight parents of the NIAB MAGIC wheat population (Mackay *et al*., 2014), for variation in RSA and growth dynamics at seedling establishment. MAGIC populations have higher diversity than previous types of mapping populations, and enable rapid identification of gene regions associated with phenotypes (Arrones *et al*., 2020). Winter wheat is a major source of food security and merits phenotyping and genotyping in soils because it has been studied less because of its long season compared to spring wheats. We provide an approach to phenotyping RSA in natural soil at a medium throughput in 4D using MRI, and quantify the relative importance of root emergence, elongation and angle as quantitative traits underlying RSA phenotypes to speed up breeding for productive establishment.

Methods

Wheat genotypes

The eight parent lines of the NIAB MAGIC population of winter wheat (*Triticum aestivum* L. vars Alchemy, Brompton, Claire, Hereward, Rialto, Robigus, Soissons, Xi 19) were used in the study (MacKay *et al*., 2014). Seeds were provided by BASF, and had received fungicide treatment (Raxil MD).

Plant growth conditions

To ensure comparable seed quality, age and reserve, all genotypes were multiplied in the previous generation at the same time in the same compartment. All experiments were carried out within 2 months. Seeds of each wheat genotype (36 seeds each) were germinated in a Petri dish on wet filter paper kept in a light-tight box in a climate chamber (16 h/8 h day/night with temperature of 20°C/16°C) for 24 h. Seedlings were selected by eye for homogeneity, with the coleoptile 2 mm long

and the primary seminal root visible but not elongated, and transplanted to the growth and imaging container (Fig. S1).

The plant growth and imaging container was custom made to enable medium throughput phenotyping. It consisted of a stack of four pots (PVC tubes of 12.5 cm outer diameter, 11.3 cm inner diameter, 12 cm height) designed to fit into the MRI radio frequency coil (Fig. S1). We used a commercially available field soil (loamy sand, sieved to 2mm, brand name Sp2.1, Landwirtschaftliche Untersuchungs- und Forschungsanstalt Speyer, Speyer, Germany; for details on the used soil see Pflugfelder *et al.*, 2017 and the vendor's homepage). The soil was dried down and strong ferromagnetic particles were removed (ferromagnetic particle content: 2.5% m/m, Pflugfelder *et al.* 2017). After rewetting the soil to a moisture of 6.8% (m/m), 1.18kg was filled in each pot and compressed to a soil column of 9cm height by tapping the pot onto the table, leading to a homogeneous distribution of the soil inside the pot (Fig. S1, C)) with a bulk density of 1.22 kg/L. After seeding, an additional 40ml of water as applied, resulting in a final moisture of 13.3% (v/v) which corresponds to 42% of the water holding capacity of the soil (Pflugfelder *et al.*, 2017).

Seedlings were planted with the primary root facing downwards at 1.5 cm depth in a hexagonal grid with 2.5 cm distance between seedlings (Fig. S1). To avoid genotype interactions, each genotype was grown in a separate pot. Similar evaporation conditions were maintained by sealing the pot at the top of the stack with a PVC lid and the others with parafilm. Stable temperature conditions were maintained by keeping the stack inside the MRI bore during the whole experiment. Temperature inside the MRI bore was controlled by inflow of climatized air into the MRI bore, leading to soil temperatures of 16°C and air temperature above the pots of 17°C without MRI scanning.

Seedlings were grown and imaged in soil for three days. Images of emerging roots were acquired by MRI every 6 h, leading to a total of twelve 3D data sets per pot per experimental run (image analysis given below). After the last MRI measurement, seedlings were harvested and total root length was determined by scanning, using WinRhizo software (WinRhizo 2012, Regent Instruments, Canada). Per experimental run, four pots and thus four genotypes were measured.

The custom container of stacked pots combined with the continuous imaging within the MRI bore resulted in a throughput of 72 seedlings and 4 genotypes per experimental run (1 genotype per pot * 4 pots * 18 seedlings per pot = 72 seedlings and 4 genotypes over 4 days (1 day germination and 3 days measurements in the MRI) and 12 imaging time points). The throughput can be greater if the plants are climatized outside the MRI bore (Table 1).

MRI measurements

Measurements were performed in a 4.7 T vertical magnet (Magnex, Oxford, UK) equipped with a Varian console (Varian, Palo Alto, CA, USA). For details of the measuring system, see van Dusschoten *et al*., 2016. Briefly, a 140 mm birdcage RF coil (Doty Scientific Inc, Columbia, SC, USA) was used. Images were acquired using a vendor-supplied spin echo multi slice (SEMS) sequence with the following parameters: TE = 7 ms, TR = 2.5 s, 120 slices, resolution 0.55 x 0.55 x 1.0 mm^3, field of view 121 x 121 x 120 mm^3, 2 averages, bandwidth = 156 kHz, measurement time: 18.3 min. The measurement of the individual pots was automated using an industrial pick-and-place robot (Mini-Liner 3.0 Alu; Geiger Handling, Jülich, Germany).

Data analysis

MRI time series were analyzed using NMRooting (van Dusschoten *et al*., 2016). For each seedling, the root system of the last measurement was manually delineated. For earlier time points, the root structure was automatically obtained as follows: The endmost root structure was overlaid on the image of the previous time point. As the roots on the previous time point are expected to be shorter or the same, the tips were traced back up to the point where root signal was again detected in the image. The root structure was cropped to this position and the process was repeated until the root structure for all 12 time points was extracted. In rare cases where this automatic extraction failed, the root structure was selected manually for each timepoint. To ease manual delineation, an automatic filter was applied to mask out most of the root systems of the other seedlings in the pot. At the final growth stages acquired, the wheat seedlings had a maximum of 5 seminal axile roots, with the first root

emerging as single (primary) seminal axile root, and the others emerging in pairs from the seed. The roots were labeled manually and classified as 'primary root', 'first seminal pair' and 'second seminal pair'. The segmentation process is depicted in Fig. 2. To process all 12 measurement time points of a seedling took between 2 to 10 min, depending on the amount of manual intervention needed.

From the extracted root structure, phenotypic traits measured were: individual root lengths, total root length, emergence root angle (calculated relative to the vertical axis at a distance of 2 cm from the seed, omitting roots that touched pot edge within 2 cm or were shorter than 2 cm), maximal root system width, maximal root system depth, and the time of root and coleoptile emergence from soil. The measured traits are depicted in Fig. 2C and D. As small parts of the segmented root occasionally overlapped with the seed volume, a root was not considered as emerged unless it reached a length of at least 8 mm.

Statistical analysis

Four independent experimental runs were conducted. In each run, four parent lines were included such that each of the eight parent lines was measured in two independent experimental runs with N = 18 seedlings per run. The data of both runs were pooled (for discussion see supplemental data), leading to a total of N = 36 replicates per genotype. In each run 3D volumes were acquired at 12 time points. Each 3D volume contained all 18 seedlings of one genotype which were analyzed independently. In total 288 seedlings were analyzed and a total of 192 3D volumes acquired. Due to the measurement time needed to acquire the 3D volumes, phenotypes were obtained at slightly shifted time points. For comparisons between parents, phenotypes were linearly interpolated to common time points and then compared by pairwise t-test for each phenotype with $p < 0.05$ considered significant. The Bonferroni correction was applied to account for the effects of multiple testing (Sedgwick, 2012). Non-germinated seeds, roots which did not emerge or root angles that could not be quantified due to pot constraints were excluded from statistical analyses.

Results

Throughput and repeatability of MRI-based root phenotyping

The MRI phenotyping workflow is based on 12 scans of the pot stack over a period of three days. Due to the automated robotic arm images could be acquired fully automated every 6 hours. 72 plants per experimental run (18 plants per pot) could be analysed because of the stacked pot design (Table 1). At harvest, several roots already touched the pot bottom and multiple coleoptiles reached the soil surface (Fig. 1). The time-resolved image sequence allowed observation of root growth dynamics (see a typical time series over an experimental run for genotype 'Claire' in the movie S1). Root lengths obtained from the final MRI images were highly correlated to root lengths obtained from the respective seedlings by destructive harvests immediately after the MRI experiments (see Fig. S2), with a correlation of 0.98 of the non-destructive MRI method to the method of washing and flatbed scanning roots using WinRhizo.

To ensure stable temperature conditions we kept the pots in the climatized MRI bore during the whole experiment. We repeated the experiment twice to investigate the repeatability of the proposed MRI workflow. Fig. S3 shows the comparison of 12 traits for the 8 genotypes at the final growth stage acquired for both experiments. 88 out of these 96 comparisons did not show a significant deviation, indicating a good but not perfect repeatability of the growing conditions while the stacked pots remained in the bore for scanning over 3 days. This optimization strategy, however, limited the achievable plant throughput as the MRI machine was idle for 78% of the time (see Table 1).

Root phenotypes extracted using MRI workflow

The total root lengths, elongation rates, depths and widths differed significantly among the eight parent lines (Figs 3, 4 and 5). The time and space-resolved MRI workflow enabled extraction of the quantitative parameters of the individual axile roots of the seminal root system: primary, first pair and second pair.

Emergence timing of seminal roots

The individual roots within a seminal root pair (first and second pair after the primary root) emerged at a similar time (84% of individuals in pairs emerged within 6 hours of each other). The mean emergence times of the pairs, however, differed among the genotypes (Fig. 3). A particularly clear effect was found for the emergence of the first seminal root pair, which was 10 h earlier in genotypes Claire and Hereward than the other genotypes, suggesting a mechanism common to these two genotypes. The first seminal root pair in Claire and Hereward was longer than in the other genotypes over the complete measurement duration (Fig. 4C), but not the second seminal pair, which was shorter in Claire and Hereward than in other genotypes (Fig. 4B, D). Soissons had the slowest primary root growth and latest emerging first seminal pair, leading to the shortest total root length at harvest for this genotype.

Elongation rates of seminal roots

Total root system lengths fell into three types: fast elongating (Robigus, Hereward and Claire), medium elongating (Alchemy, Brompton, Rialto, Xi 19) and slow elongating (Soissons) (Fig. 4). Total root lengths were reached through different rates of growth of the individual axile roots of the genotypes (Fig. S5). For example, Claire and Hereward had a similar total root length and length of first seminal pair, but Claire had a reduced primary root growth and earlier emergence of the second seminal pair than Hereward. Soissons showed almost no primary root growth, but fast first and second seminal root pair growth, resulting in the highest root length of the second seminal pair at harvest of the eight parents. In contrast, Robigus had the fastest-growing primary root, but the first seminal root pair developed slowly, and the second seminal root pair even more slowly.

Root angles

The emergence root angles of the first seminal root pair are shown in Fig. 6. We identified two groups: a steep (Alchemy, Brompton, Claire and Hereward; mean angle 36°) and a more shallow angle (Rialto, Robigus, Xi 19; mean angle 43°) group.

Root distribution in width and depth

We used root depth distributions (Fig. 5), 2D trajectory plots of root width and depth (Fig. 7A) and primary and seminal root pair lengths (Fig. 7B) to resolve the quantitative growth traits underlying RSA. The depth distribution of the root lengths (Fig. 5) varied most between the genotypes Robigus and Soissons. This was related to Robigus having the longest primary root of all investigated genotypes (Fig. 5B), and Soissons having the shortest primary root, shortest first primary root pair (Fig. 5C) and the longest second primary root pair (Fig. 5D). Despite its shallow emergence root angle (Fig. 6), Robigus developed the deepest root system compared to its width of all parent lines (Fig. 7A). This was realized by a delayed elongation of the first seminal root pair relative to its primary root (Fig. 7B). The fastest elongation rates were found in Soissons, followed by Claire (Fig. 7B). This relationship between primary root and second seminal root pair growth continued through the experiment (Fig. 7B).

Discussion

The unexpected finding from the 4D MRI phenotyping was the importance of variation in seminal root elongation rates in root system architecture among the MAGIC genotypes. More specifically, differences in the timing of elongation between the primary and first and second pair of seminal roots appears to be a trait underlying RSA which can be more important than the emergence root angle for the resulting root system depth and width. The highly dynamic MRI workflow applied in this study to seedlings in soil, with plant neighbors as in a field scenario, was essential to identifying and quantifying this phenotype. We discuss the phenotype and the new MRI workflow in detail with a view for future applications to genetic improvement of wheat.

Discovery of mechanisms regulating root system architecture

Root system architecture is determined by three plant characteristics, namely the angles of the roots, the growth rates of the roots, the number of roots (Lynch, 1995), and additionally by the environment (Rich and Watt, 2013). Selection for root system architecture has had substantial focus on root angle

as the key quantitative trait, or "proxy" to use in higher throughput pre-breeding programs (e.g., Liao *et al*., 2004; Uga *et al*., 2011; Richard *et al*., 2015). A range of phenotyping techniques are available for quantifying root angles; notably in agar, papers and in baskets. However, recent studies showed that the root phenotypes measured using these artificial substrates do not strongly correlate with final root system depths for wheat in the field (Rich *et al*., 2020), regardless if measuring the first or second seminal root pair at the seedling stage.

In our study, the trait trajectory plots revealed independent and time-resolved expression of phenotypes of the primary and seminal root pairs allowing us to see the association of the separate aspects of root system architecture: angle, elongation and root type (Fig. 7A). The results suggest that root elongation rate and the timing of emergence of the root can be more important than basal root angles for determining the width and depth of the root system, especially for early growth phases. For future phenotyping for root system architecture we recommend quantification of elongation rates, numbers of axile roots and their relative appearances.

It is possible that the soil type and planting we used as well as the 3D quantification method revealed phenotypes not yet quantified in conventional methods. In our method we analyzed multiple seedlings within one pot. This approach mimics the actual field situation, where plants are close and develop the root system in 3D with neighbors. It contrasts to conventional phenotyping approaches that either use single plants in one pot or multiple plants grown in a 2D plane with or without soil. Using neighboring plants, effects of planting density or interaction between roots from different plants can be quantified. During the very early plant stage of the two experiments conducted here roots of the seedlings were still well separated, suggesting that competition for resources such as space, water and nutrients was not yet influencing direction of growth. Overlapping roots were only observed at the pot walls. In each pot, six seedlings were planted directly at the pot wall (Fig. S1). To investigate the effect of the seedling position on the extracted traits we compared these six outer seedlings to the remaining twelve inner seedlings for each genotype and trait (Fig. S4). Due to constraints of the pot wall, for some genotypes the maximal root system width at harvest of the outer seedling was

significantly smaller compared to the inner seedlings. For all other traits, however, we did not find significant differences due to seedling position.

The NIAB MAGIC parents and their progeny could be used to untangle the genetics regulating angle, elongation and emergence time of roots. For some traits such as the emergence root angle of the first seminal root pair (Fig. 6), the genotypes are clustered into groups with remarkably similar phenotypic values, suggesting that these traits are controlled to a large degree by shared genes. However, despite sharing similar root angles, the genotypes expressed contrasting growth patterns. For example three genotypes had large emergence root angles which is typically expected to result in a shallower root system (Lynch, 2013). While two of these genotypes (Xi 19 and Rialto) showed the expected behavior the third (Robigus) had the largest root system depth compared to its width of all investigated genotypes (Fig. 7A). The phenotype of Robigus can be explained by variation in the growth rates of the primary and seminal root types relative to each other (Fig. 7B). The mechanisms regulating the variation in emergence timing and elongation of the primary relative to seminal root pairs has so far not been investigated to our knowledge.

The novel MRI workflow allows phenotyping of seedlings in medium throughput

The temporal and spatial resolution of the 3D root architecture of the NIAB MAGIC parents was achieved by using a non-invasive MRI workflow with medium throughput. It was achieved for young establishing roots and coleoptiles by combining three aspects. First, we overcame the single plant phenotyping by studying multiple seedlings in stacked soil-filled pots simultaneously (Fig. S1). Second, the automated robotic system (Dusschoten *et al*., 2016) allowed to repeatedly scan the pot stack while it remained within the bore of the MRI machine and in stable temperature conditions. Third, image analysis, notably 2D trait trajectory plots, allowed extraction of static and time resolved traits (Table 1). With this approach the dynamics of the root system for seedling establishment, a critical phase in the plant growth cycle, was analyzed in natural soils with the aim to validate this approach for pre-breeding and possibly breeding.

The throughput was achieved by tailoring the experiment to the seed establishment phase up to the shoot emergence from the soil. This allowed throughput optimizations by using a high seeding density (1795 seeds/m^2 compared to typical values of 250-300 seeds/m^2 (Spink *et al.*, 2000)) and growing the seeds in the dark. The importance of plant traits extracted in this early growth phase for mature plants and yield needs to be established in separate experiments where seeding densities and light conditions need to be adapted. Throughput was limited to 4 pots with 18 seedlings each, leading to a throughput of 72 seedlings measured continuously for almost 3 days (Table 1). The limiting factor was the need to keep the stack of pots inside the temperature controlled MRI bore for the complete experiment. This can be overcome in future when using controlled conditions outside the MRI bore, potentially increasing the throughput to a continuous measurement of 18 pots, and a total of 324 seedlings per experimental run. Further increase of plant throughput might be realized by reducing the measurement time for a single pot or by increasing the time between two measurements of the same pot. If only a single image per seedling is desired, up to 1296 seedlings per day could be imaged with the proposed protocol, developing MRI for seed establishment to a high throughput phenotyping method.

Future applications

The throughput achievable with MRI as demonstrated in this study has the potential to be used in phenotype-assisted pre-breeding or breeding (Watt *et al.*, 2020). Pre-breeding includes research to identify quantitative trait loci (QTL), which are then used to identify gene regions strongly associated with phenotypes to select in breeding using marker assisted selection. The NIAB winter wheat population was developed for QTL discovery, and QTLs linked to leaf senescence and plant height (Camargo *et al.*, 2016), presence of awns (Mackay *et al.*, 2014), resistant to *Septoria tritici* (Riaz *et al.*, 2020), and leaf and glume blotch (Lin *et al.*, 2020) were detected in the NIAB population. Large variation may be discovered among the progeny due to transgressive segregation, increasing the chances of identifying QTL. The MRI platform could be scaled to phenotype a subset of the NIAB MAGIC progeny.

The high cost and technical complexity of MRI makes it challenging, however MRI allows for non-destructive 3D measurements of seedling roots in natural soil, compared to other methods that image roots in 2D or after digging and washing. Further, it has the advantages over other 3D methods of using biologically-safe and non-ionizing radiation compared to other methods (Wasson *et al*., 2020), while retaining a similar root resolving power as X-ray CT (Metzner *et al*., 2015). There are collaboration mechanisms which allow users to get access to the MRI facility at Forschungszentrum Jülich (Pieruschka and Schurr, 2019) to identify genetic variation in establishment of root and shoot traits across a wide range of crop and native plant species.

The MRI platform can not only be scaled up in plant number but can be used also to discover the role of soil environment in root system architecture variation. The natural soil used in this study results in realistic mechanical stress to the roots to enable investigations of the effect of various mechanical resistances either by varying the soil type or by using different soil compaction. Also other research questions such as the influence of the rhizosphere microbiome or the effect of drought are best studied in natural soils. Thereby our approach may help understanding differences and similarities between plants growing in controlled conditions and in the field in high temporal and spatial resolution.

Supplementary data description:

Fig. S1: Experimental setup

Fig. S2: Comparison of root length obtained by MRI and destructive harvest.

Fig. S3: Repeatability of measured traits over two experiments

Fig. S4: Influence of seedling position on extracted traits

Fig. S5: Development of growth rates for the individual root classes

Movie S1: 3D visualization of complete growth cycle over one experiment (genotype: Claire).

Acknowledgements:

We are grateful to Esther Breuer for helping to conduct the MRI image analysis. This work was supported by BASF SE. Prof. Michelle Watt holds the Adrienne Clarke Chair of Botany, which is supported through the University of Melbourne Botany Foundation. We are grateful for the provision of MAGIC parents by NIAB.

Author contributions:

Conceptualization: DVD, DP, MW, SJ, RK, HF, KAN

Methodology: DVD, JK, DP, SJ

Investigation: DP, CM, HF

Formal Analysis: DP

Writing – original draft: DP

Writing – review & editing: DP, MW, RK, KAN, SP, HF

Project administration: MW, RK, KAN

Data availability statement:

The data supporting the findings of this study are available from the corresponding author (Daniel Pflugfelder), upon request.

References:

Arrones A, Vilanova S, Plazas M, Mangino G, Pascual L, Díez MJ, Prohens J, Gramazio P. 2020. The Dawn of the Age of Multi-Parent MAGIC Populations in Plant Breeding: Novel Powerful Next-Generation Resources for Genetic Analysis and Selection of Recombinant Elite Material. Biology **9**, 229.

Atkinson JA, Pound MP, Bennett MJ, Wells DM. 2019. Uncovering the hidden half of plants using new advances in root phenotyping. Current Opinion in Biotechnology **55**, 1–8.

Blaser SRGA, Schlüter S, Vetterlein D. 2018. How much is too much?—Influence of X-ray dose on root growth of faba bean (Vicia faba) and barley (Hordeum vulgare). PLOS ONE **13**, e0193669.

Blunk S, Hafeez Malik A, de Heer MI, Ekblad T, Fredlund K, Mooney SJ, Sturrock CJ. 2017. Quantification of differences in germination behaviour of pelleted and coated sugar beet seeds using x-ray computed tomography (x-ray CT). Biomedical Physics & Engineering Express **3**, 044001.

Camargo AV, Mott R, Gardner KA, Mackay IJ, Corke F, Doonan JH, Kim JT, Bentley AR. 2016. Determining Phenological Patterns Associated with the Onset of Senescence in a Wheat MAGIC Mapping Population. Frontiers in Plant Science **7**, 1540.

Clowes FAL, Hall EJ. 1963. The quiescent centre in root meristems of Vicia faba and its behaviour after acute X-irradiation and chronic gamma irradiation. Radiation Botany **3**, 45–53.

Consortium (IWGSC) TIWGS, Appels R, Eversole K, *et al.* 2018. Shifting the limits in wheat research and breeding using a fully annotated reference genome. Science **361**, 661.

de Dorlodot S, Bertin P, Baret P, Draye X. 2005. Scaling up quantitative phenotyping of root system architecture using a combination of aeroponics and image analysis. Aspects of Applied Biology **73**, 41–54.

van Dusschoten D, Metzner R, Kochs J, Postma JA, Pflugfelder D, Buehler J, Schurr U, Jahnke S. 2016. Quantitative 3D Analysis of Plant Roots growing in Soil using Magnetic Resonance Imaging. Plant Physiology **170**, 1176–1188.

Flavel RJ, Guppy CN, Tighe M, Watt M, McNeill A, Young IM. 2012. Non-destructive quantification of cereal roots in soil using high-resolution X-ray tomography. Journal of Experimental Botany **63**, 2503–2511.

Gioia T, Galinski A, Lenz H, *et al.* 2016. GrowScreen-PaGe, a non-invasive, high-throughput phenotyping system based on germination paper to quantify crop phenotypic diversity and plasticity of root traits under varying nutrient supply. Functional Plant Biology **44**, 76–93.

Van Harsselaar JK, Claußen J, Lübeck J, Wörlein N, Uhlmann N, Sonnewald U, Gerth S. 2021. X-Ray CT Phenotyping Reveals Bi-Phasic Growth Phases of Potato Tubers Exposed to Combined Abiotic Stress. Frontiers in Plant Science **12**, 541.

Henry A, Chaves NF, Kleinman PJA, Lynch JP. 2010. Will nutrient-efficient genotypes mine the soil? Effects of genetic differences in root architecture in common bean (Phaseolus vulgaris L.) on soil phosphorus depletion in a low-input agro-ecosystem in Central America. Field Crops Research **115**, 67–78.

Huang BE, Verbyla KL, Verbyla AP, Raghavan C, Singh VK, Gaur P, Leung H, Varshney RK, Cavanagh CR. 2015. MAGIC populations in crops: current status and future prospects. Theoretical and Applied Genetics **128**, 999–1017.

International Commission on Non-Ionizing Radiation Protection (ICNIRP). 2017. ICNIRP Statement on Diagnostic Devices Using Non-ionizing Radiation: Existing Regulations and Potential Health Risks. Health Physics **112**, 305–321.

Khalil AM, Murchie EH, Mooney SJ. 2020. Quantifying the influence of water deficit on root and shoot growth in wheat using X-ray Computed Tomography. AoB PLANTS **12**.

Liao H, Yan X, Rubio G, *et al.* 2004. Genetic mapping of basal root gravitropism and phosphorus acquisition efficiency in common bean. Functional Plant Biology **31**, 959–970.

Lin M, Corsi B, Ficke A, Tan K-C, Cockram J, Lillemo M. 2020. Genetic mapping using a wheat multi-founder population reveals a locus on chromosome 2A controlling resistance to both leaf and glume blotch caused by the necrotrophic fungal pathogen Parastagonospora nodorum. Theoretical and Applied Genetics **133**, 785–808.

Lynch J. 1995. Root Architecture and Plant Productivity. Plant Physiology **109**, 7–13.

Lynch JP. 2013. Steep, cheap and deep: an ideotype to optimize water and N acquisition by maize root systems. Annals of Botany **112**, 347–357.

Mackay IJ, Bansept-Basler P, Barber T, *et al.* 2014. An Eight-Parent Multiparent Advanced Generation Inter-Cross Population for Winter-Sown Wheat: Creation, Properties, and Validation. Genes|Genomes|Genetics **4**, 1603–1610.

Manschadi AM, Christopher J, deVoil P, Hammer GL. 2006. The role of root architectural traits in adaptation of wheat to water-limited environments. Functional Plant Biology **33**, 823–837.

Mawodza T, Burca G, Casson S, Menon M. 2020. Wheat root system architecture and soil moisture distribution in an aggregated soil using neutron computed tomography. Geoderma **359**, 113988.

Metzner R, Eggert A, van Dusschoten D, Pflugfelder D, Gerth S, Schurr U, Uhlmann N, Jahnke S. 2015. Direct comparison of MRI and X-ray CT technologies for 3D imaging of root systems in soil: potential and challenges for root trait quantification. Plant Methods **11**, 17.

Mooney SJ, Pridmore TP, Helliwell J, Bennett MJ. 2012. Developing X-ray Computed Tomography to non-invasively image 3-D root systems architecture in soil. Plant and Soil **352**, 1–22.

Nagel KA, Lenz H, Kastenholz B, *et al.* 2020. The platform GrowScreen-Agar enables identification of phenotypic diversity in root and shoot growth traits of agar grown plants. Plant Methods **16**, 89.

Nagel KA, Putz A, Gilmer F, *et al.* 2012. GROWSCREEN-Rhizo is a novel phenotyping robot enabling simultaneous measurements of root and shoot growth for plants grown in soil-filled rhizotrons. Functional Plant Biology **39**, 891–904.

Ober ES, Alahmad S, Cockram J, *et al.* 2021. Wheat root systems as a breeding target for climate resilience. Theoretical and Applied Genetics **134**, 1645–1662.

Palta J, Watt M. 2009. Chapter 13 - Vigorous Crop Root Systems: Form and Function for Improving the Capture of Water and Nutrients. In: Sadras V, Calderini D, eds. Crop Physiology. San Diego: Academic Press, 309–325.

Perkins AC, Lynch JP. 2021. Increased seminal root number associated with domestication improves nitrogen and phosphorus acquisition in maize seedlings. Annals of Botany **128**, 453–468.

Pflugfelder D, Metzner R, van Dusschoten D, Reichel R, Jahnke S, Koller R. 2017. Non-invasive imaging of plant roots in different soils using magnetic resonance imaging (MRI). Plant Methods **13**, 102.

Pieruschka R, Schurr U. 2019. Plant Phenotyping: Past, Present, and Future. Plant Phenomics **2019**, 7507131.

Riaz A, KockAppelgren P, Hehir JG, Kang J, Meade F, Cockram J, Milbourne D, Spink J, Mullins E, Byrne S. 2020. Genetic Analysis Using a Multi-Parent Wheat Population Identifies Novel Sources of Septoria Tritici Blotch Resistance. Genes **11**, 887.

Rich SM, Christopher J, Richards R, Watt M. 2020. Root phenotypes of young wheat plants grown in controlled environments show inconsistent correlation with mature root traits in the field. Journal of Experimental Botany **71**, 4751–4762.

Rich SM, Watt M. 2013. Soil conditions and cereal root system architecture: review and considerations for linking Darwin and Weaver. Journal of Experimental Botany **64**, 1193–1208.

Richard CA, Hickey LT, Fletcher S, Jennings R, Chenu K, Christopher JT. 2015. High-throughput phenotyping of seminal root traits in wheat. Plant Methods **11**, 13.

Sedgwick P. 2012. Multiple significance tests: the Bonferroni correction. BMJ **344**, e509.

Shiferaw B, Smale M, Braun H-J, Duveiller E, Reynolds M, Muricho G. 2013. Crops that feed the world 10. Past successes and future challenges to the role played by wheat in global food security. Food Security **5**, 291–317.

Spink JH, Semere T, Sparkes DL, Whaley JM, Foulkes MJ, Clare RW, Scott RK. 2000. Effect of sowing date on the optimum plant density of winter wheat. Annals of Applied Biology **137**, 179–188.

Trachsel S, Kaeppler SM, Brown KM, Lynch JP. 2011. Shovelomics: high throughput phenotyping of maize (Zea mays L.) root architecture in the field. Plant and Soil **341**, 75–87.

Tracy SR, Black CR, Roberts JA, Sturrock C, Mairhofer S, Craigon J, Mooney SJ. 2012. Quantifying the impact of soil compaction on root system architecture in tomato (Solanum lycopersicum) by X-ray micro-computed tomography. Annals of Botany **110**, 511–519.

Tracy SR, Nagel KA, Postma JA, Fassbender H, Wasson A, Watt M. 2020. Crop Improvement from Phenotyping Roots: Highlights Reveal Expanding Opportunities. Trends in Plant Science **25**, 105–118.

Tuberosa R, Sanguineti MC, Landi P, Michela Giuliani M, Salvi S, Conti S. 2002. Identification of QTLs for root characteristics in maize grown in hydroponics and analysis of their overlap with QTLs for grain yield in the field at two water regimes. Plant Molecular Biology **48**, 697–712.

Uga Y, Okuno K, Yano M. 2011. Dro1, a major QTL involved in deep rooting of rice under upland field conditions. Journal of Experimental Botany **62**, 2485–2494.

Wasson AP, Nagel KA, Tracy S, Watt M. 2020. Beyond Digging: Noninvasive Root and Rhizosphere Phenotyping. Trends in Plant Science **25**, 119–120.

Watt M, Kirkegaard JA, Rebetzke GJ. 2005. A wheat genotype developed for rapid leaf growth copes well with the physical and biological constraints of unploughed soil. Functional Plant Biology **32**, 695–706.

Watt M, Moosavi S, Cunningham SC, Kirkegaard JA, Rebetzke GJ, Richards RA. 2013. A rapid, controlled-environment seedling root screen for wheat correlates well with rooting depths at vegetative, but not reproductive, stages at two field sites. Annals of Botany **112**, 447–455.

Watt M, Fiorani F, Usadel B, Rascher U, Muller O, Schurr U. 2020. Phenotyping: New Windows into the Plant for Breeders. Annual Review of Plant Biology **71**, 689–712.

York LM, Lynch JP. 2015. Intensive field phenotyping of maize (Zea mays L.) root crowns identifies phenes and phene integration associated with plant growth and nitrogen acquisition. Journal of Experimental Botany **66**, 5493–5505.

Figure legends:

Figure 1: MRI measurement (brown) of wheat seedlings (genotype: Claire) before harvest (92h after sowing). To improve visualization the grey outline of the pot was added in post processing. The lower end of the transparent ring marks the soil surface. MRI data is showing seedling roots, seeds and coleoptiles. Guttation droplets can be observed at the tip of selected coleoptiles. Undesired MRI signal includes condensation water visible at the pot walls and germinating weed seeds throughout the soil. The complete growth dynamics is shown in movie S1.

Figure 2: Data processing steps. (A) A MRI image of a single pot with all 18 wheat seedlings (genotype: Alchemy) 94 h after sowing. (B) For each individual seedling, an automatically generated seedling mask can remove most of the root data from other seedlings. (C) Seedling roots are then manually delineated and labelled according to the following root categories: yellow: primary root, cyan: first seminal pair, green: second seminal pair. Still visible roots of other seedlings (grey) are not counted. Individual emergence root angles are measured against the vertical axis as depicted in red. The maximal root system depth (dashed white line) is measured from the soil surface (brown line) to the lowest root tip. (D) View from top. The maximal width is determined as the maximal extent of the root system in this view (dashed white line). Scale bar: 2 cm.

Figure 3: Emergence of primary root (top row), first seminal pair roots (middle row) and coleoptile from soil (bottom row) in hours after sowing [h a.s.]. Bar plots show mean value with one standard error, the overlaid violin plot shows the distribution of values. Groups of significant differences are depicted by lower letters. Pairwise significant difference levels are color-coded in matrix form (right column). P-values are modified with the Bonferroni correction to account for multiple testing.

Figure 4: Root length development of the eight wheat genotypes monitored in the soil up to 4 days after sowing. (A) Total root length, (B) length of primary root, (C) length of first seminal root pairs, and (D) length of second seminal root pairs. Error bars denote one standard error.

Figure 5: Root length depth profiles at harvest (94 hours after sowing). Mean values include 30 to 35 seedlings per genotype. Error bars depict one standard error of the mean. Root length density is given in mm root length per mm depth. Soil surface is at depth = 0mm.

Figure 6: Mean emergence root angles of first seminal pair as defined in Figure 2. Remarkably similar mean values are found for a steep growing group with mean angle of 36° (Alchemy, Brompton, Claire, Hereward) and a more shallow growing group at a mean angle of 43° (Rialto, Robigus, Xi 19).

Figure 7: (A) Temporal development of maximal root system width relative to maximal root system depth for the eight wheat genotypes from 26 to 94 hours after sowing. Measurements were taken every 6h. Points represent mean values, error bars one standard error of the mean. Seedlings at the pot wall were excluded. Compared to the other 7 genotypes, Robigus clearly emphasizes an early high rooting depth over a wider root system. Note that for later time points the curve is biased by roots reaching the pot bottom.

(B) Temporal development of the primary root length relative to the first seminal pair length. Five genotypes (Alchemy, Brompton, Hereward, Rialto, Xi 19) follow the same growth trajectory despite having different root length values at the individual time points. Compared to this group, two genotypes (Claire and Soissons) increase the shallow-growing first seminal root pair length, while Robigus increases the steeply growing primary root.

Tables:

Table 1. Throughput of the MRI phenotyping workflow

	Complete dataset (4 experimental runs)	Per experimental run (3 days imaging)	Maximal throughput per 24 h with continuous measurement
Individual plants	288	72	1296
Analyzed genotypes	8	4	72
Scans per plant	12	12	1
Acquired 3D volumes	192	48	72
Extracted root phenotypes	12	12	8

Figure 1

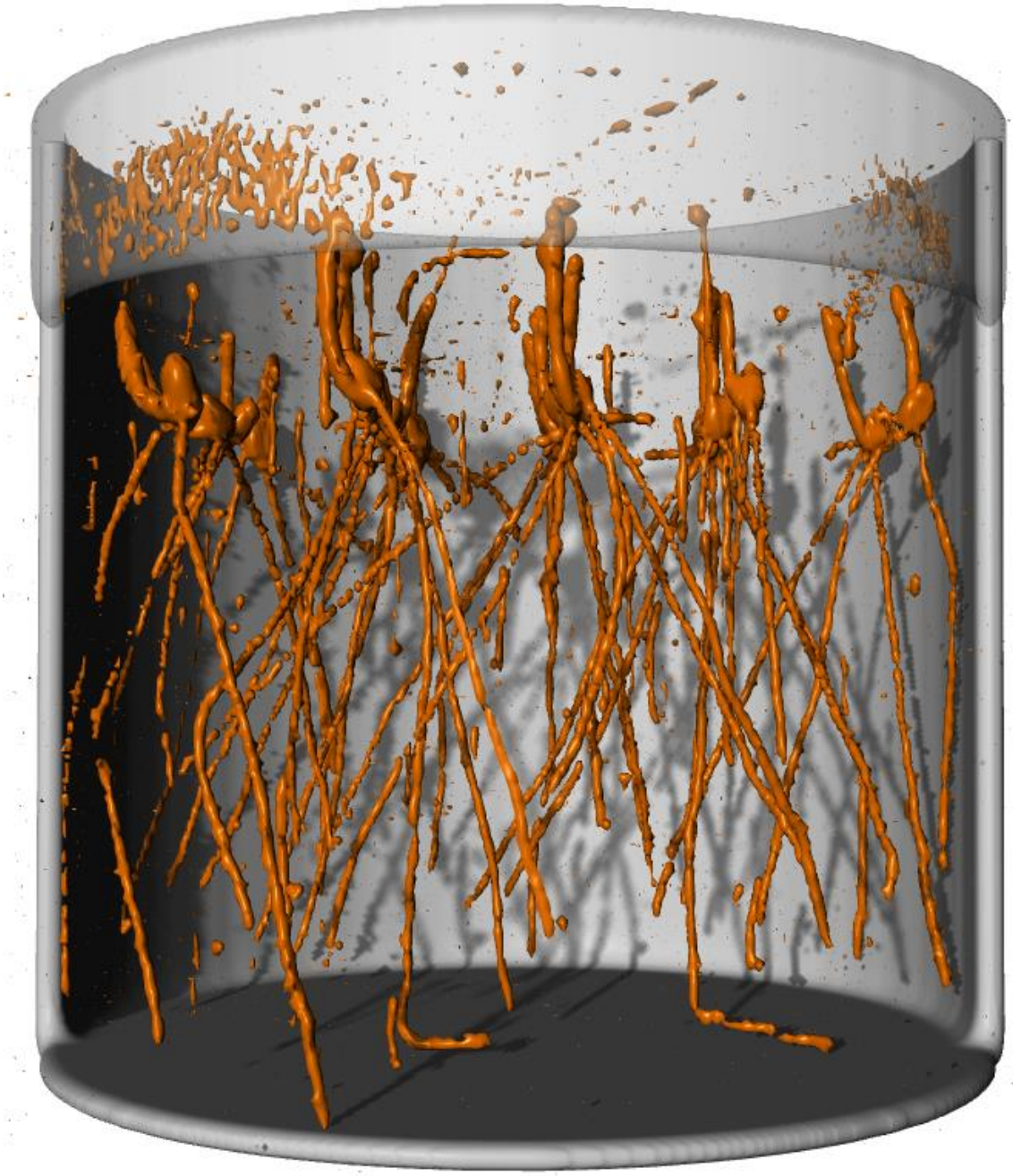

Figure 2

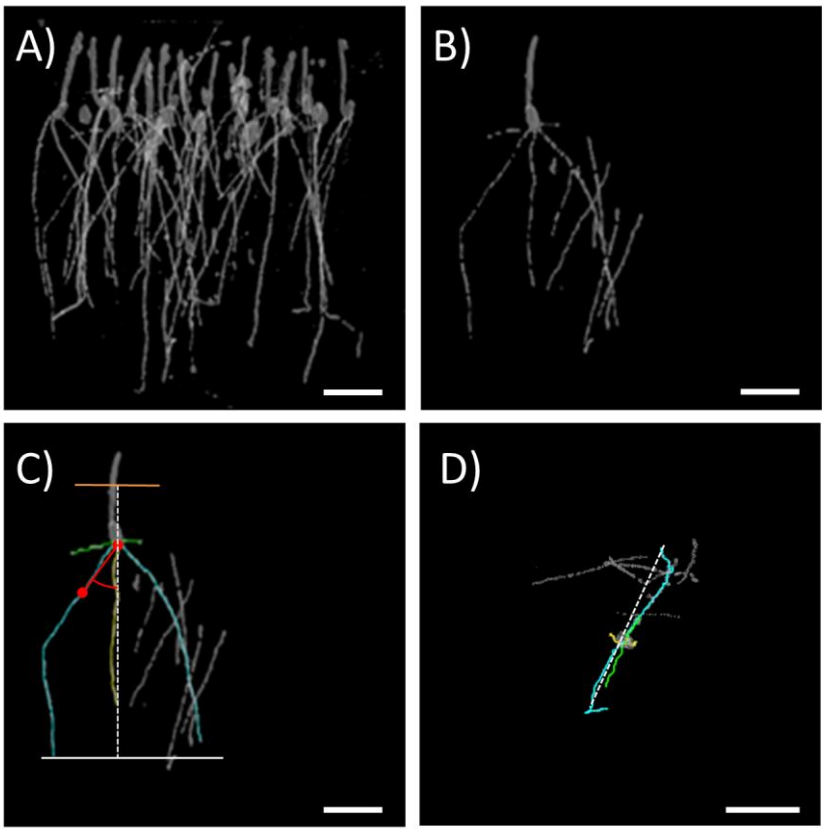

Figure 3

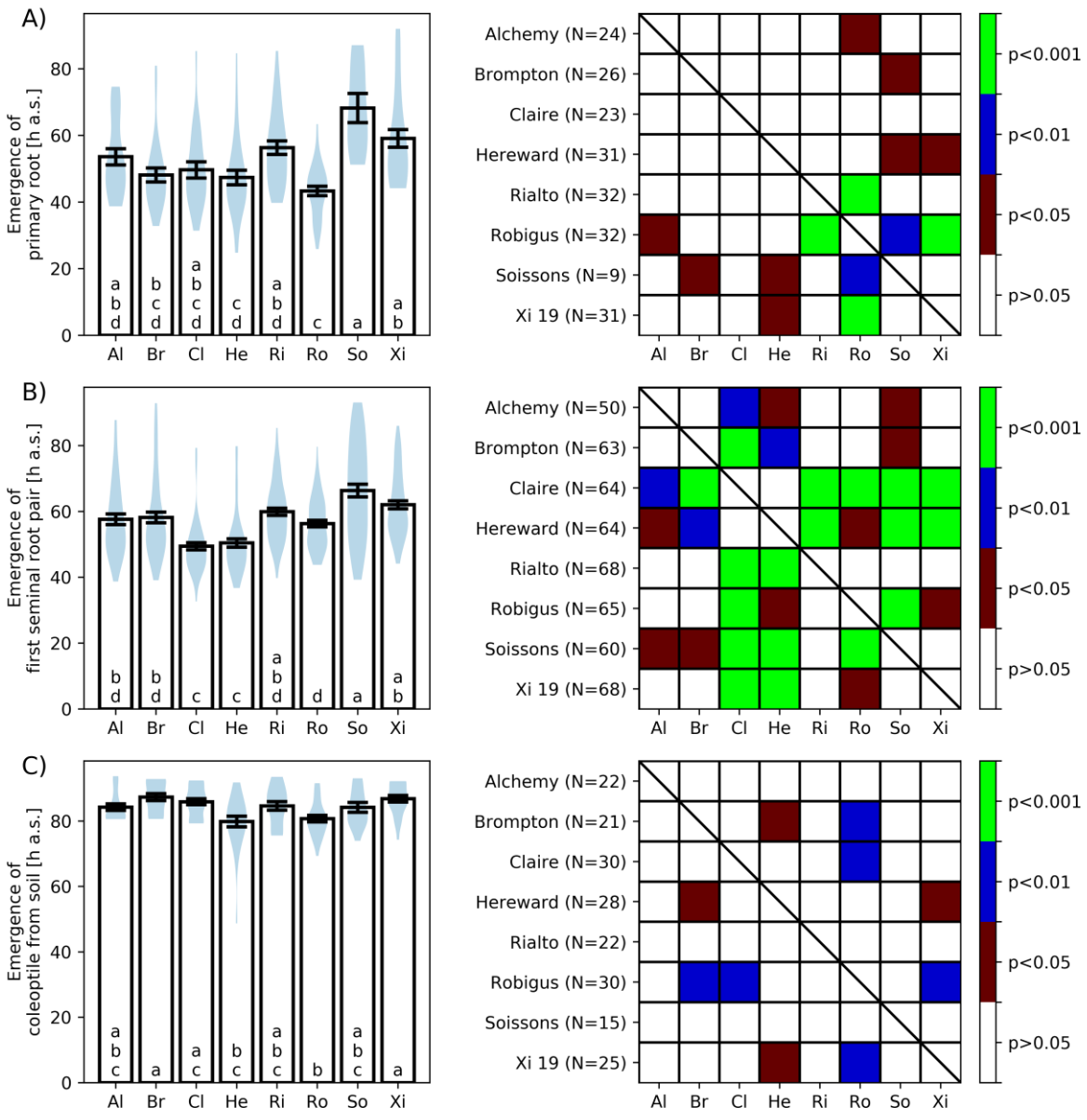

Figure 4

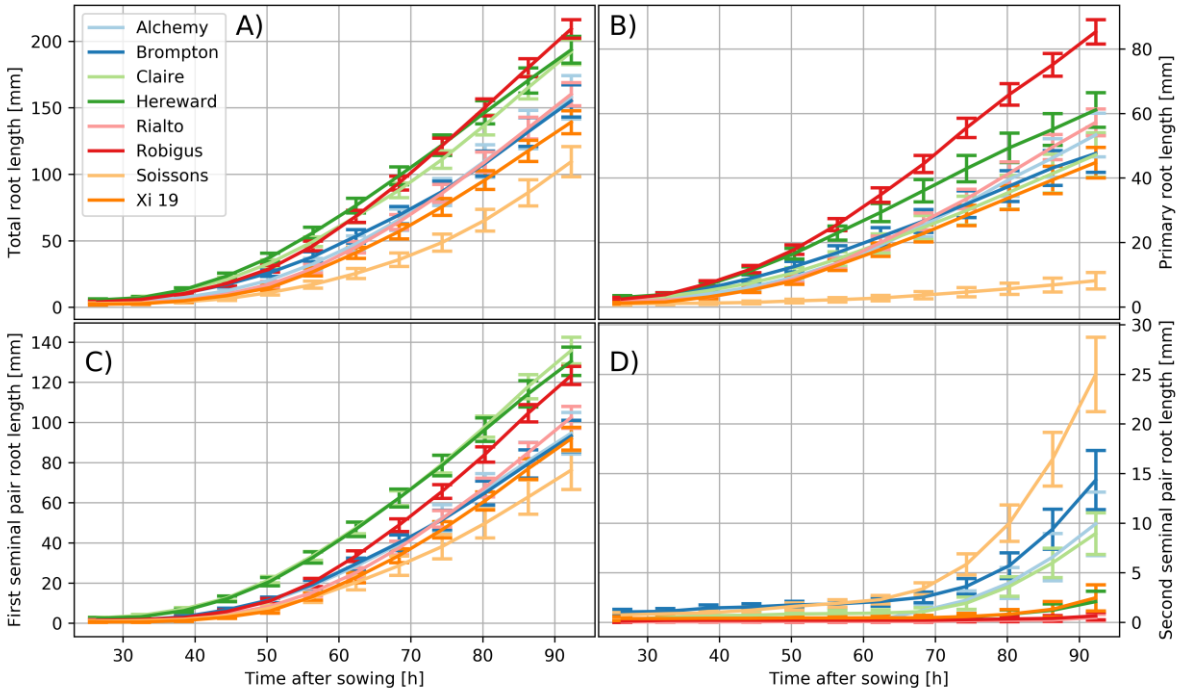

Figure 5

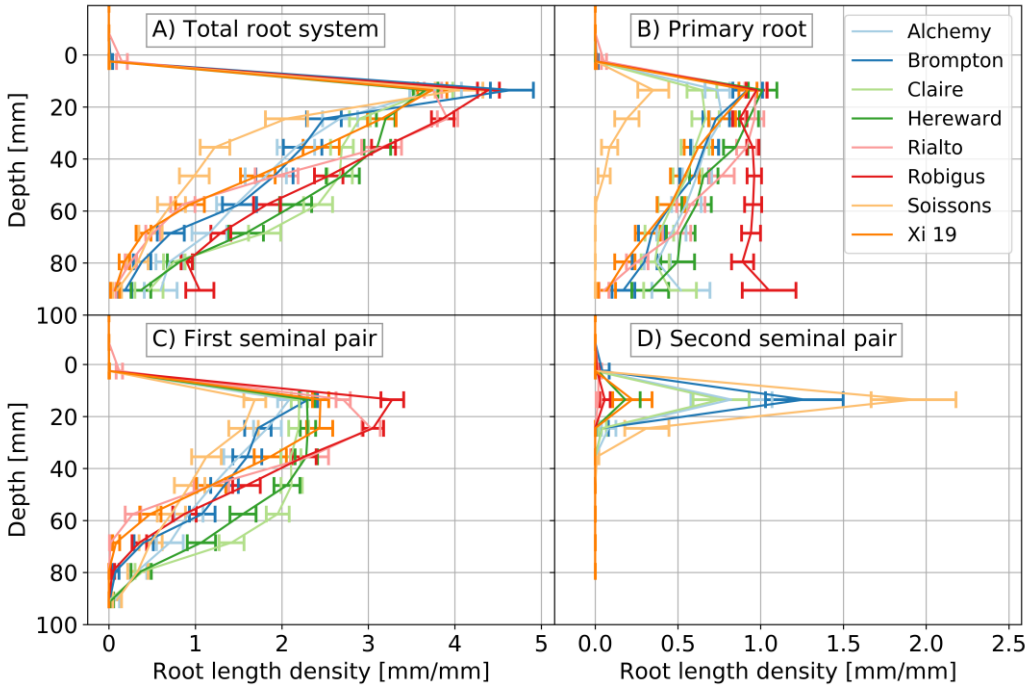

Figure 6

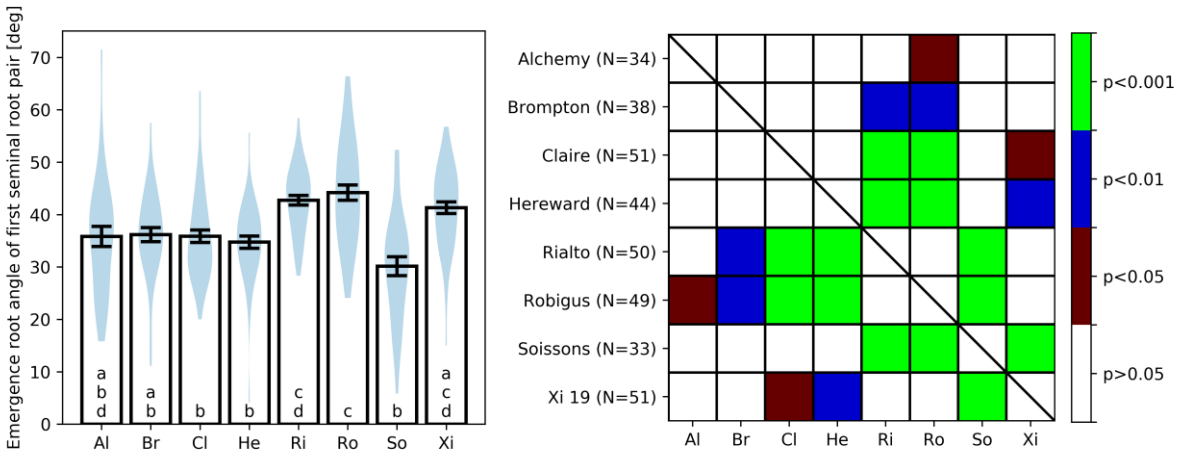

Figure 7